

RESEARCH ARTICLE

A Comparison of [^{99m}Tc]Duramycin and [^{99m}Tc]Annexin V in SPECT/CT Imaging Atherosclerotic Plaques

Yan Hu,^{1,2,3} Guobing Liu,^{1,2,3} He Zhang,^{1,2,3} Yanli Li,^{1,2,3} Brian D. Gray,⁴ Koon Y Pak,⁴ Hak Soo Choi,⁵ Dengfeng Cheng,^{1,2,3} Hongcheng Shi^{1,2,3}

¹Department of Nuclear Medicine, Zhongshan Hospital, Fudan University, No. 180, Fenglin Road, Shanghai, 200032, People's Republic of China

²Shanghai Institute of Medical Imaging, Shanghai, 200032, China

³Institute of Nuclear Medicine, Fudan University, Shanghai, 200032, China

⁴Molecular Targeting Technologies, Inc., West Chester, PA, 19380, USA

⁵Gordon Center for Medical Imaging, Department of Radiology, Massachusetts General Hospital and Harvard Medical School, Boston, MA, 02114, USA

Abstract

Purpose: Apoptosis is a key factor in unstable plaques. The aim of this study is to evaluate the utility of visualizing atherosclerotic plaques with radiolabeled duramycin and Annexin V.

Procedures: ApoE^{-/-} mice were fed with a high-fat diet to develop atherosclerosis, C57 mice as a control. Using a routine conjugation protocol, highly pure [^{99m}Tc]duramycin and [^{99m}Tc]Annexin V were obtained, which were applied for *in vitro* cell assays of apoptosis and *in vivo* imaging of atherosclerotic plaques in the animal model. Oil Red O staining, TUNEL, hematoxylin-eosin (HE), and CD68 immunostaining were used to evaluate the deposition of lipids and presence of apoptotic macrophages in the lesions where focal intensity positively correlated with the uptake of both tracers.

Results: [^{99m}Tc]duramycin and [^{99m}Tc]Annexin V with a high radiochemical purity (97.13 ± 1.52 and 94.94 ± 0.65 %, respectively) and a well stability at room temperature were used. Apoptotic cells binding activity to [^{99m}Tc]duramycin (Kd, 6.92 nM and Bmax, 56.04 mol/10¹⁹ cells) was significantly greater than [^{99m}Tc]Annexin V (Kd, 12.63 nM and Bmax, 31.55 mol/10¹⁹ cells). Compared with [^{99m}Tc]Annexin V, [^{99m}Tc]duramycin bound avidly to atherosclerotic lesions with a higher plaque-to-background ratio (P/B was 8.23 ± 0.91 and 5.45 ± 0.48 at 20 weeks, 15.02 ± 0.23 and 12.14 ± 0.22 at 30 weeks). No plaques were found in C57 control mice. Furthermore, Oil Red O staining showed lipid deposition areas were significantly increased in ApoE^{-/-} mice at 20 and 30 weeks, and TUNEL and CD68 staining confirmed that the focal uptake of both tracers contained abundant apoptotic macrophages.

Conclusions: This stable, fast clearing, and highly specific [^{99m}Tc]duramycin, therefore, can be useful for the quantification of vulnerable atherosclerotic plaques.

Key Words: Atherosclerosis, Plaque vulnerability, Duramycin, Annexin V, Phosphatidylethanolamine, Phosphatidylserine, Micro-SPECT/CT

Yan Hu and Guobing Liu contributed equally to this article.

Correspondence to: Dengfeng Cheng; e-mail: cheng.dengfeng@zs-hospital.sh.cn, Hongcheng Shi; e-mail: shi.hongcheng@zs-hospital.sh.cn

Introduction

Atherosclerotic plaque rupture is a vital hazard that leads to myocardial infarction and even sudden cardiac death [1]. Apoptosis, also known as programmed cell death, plays an important role in normal physiology and disease processes [2–5], involving the development of atherosclerosis [6, 7] and the vulnerability of atherosclerotic plaque [2]. Phosphatidylethanolamine (PE) and phosphatidylserine (PS) are established molecular markers for apoptosis [8]. PE and PS are predominantly present in the intracellular cell membrane and redistribute onto the outer surface cell membrane, which make them vital molecular indicators for cell apoptosis [9, 10].

Annexin V, a 36-kDa human protein composed of 319 amino acids, is specific to the exposed PS at a nanomolar affinity [11–14]. Therefore, radiolabeled Annexin V has been successfully used in molecular imaging to monitor apoptotic environment in many disease models including myocarditis and infective endocarditis, tumors, myocardial ischemia, and atherosclerosis [13, 15–20]. In contrast, duramycin is a low molecular weight protein (~2 kDa; 19 amino acids) and known as the smallest peptide that binds to the head group of PE with high affinity at a molar ratio of 1:1 [21–23]. Likewise, radiolabeled duramycin has also been used in tumor imaging, tissue-damage assessment after high-dose irradiation exposure, atherosclerosis, and early diagnosis of ischemia-reperfusion [9, 22–24]. However, to the best of our knowledge, the current study is the first to compare its functionality with Annexin V in evaluating atherosclerotic plaques.

In this study, we synthesized [^{99m}Tc]duramycin using a single-step radiolabeling kit and evaluated the detection capability of vulnerable atherosclerotic plaques in atherosclerosis animal models by comparing with [^{99m}Tc]Annexin V.

Materials and Methods

Ethical Statement

The animal research protocol was approved by the medical ethics committee of Zhongshan Hospital, Fudan University. All experiments were performed following the relevant guidelines and regulations of Fudan University.

Chemicals and Synthesis

Human Annexin V full length protein (Abcam, UK), single-step kit containing HYNIC-duramycin and HYNIC-linear-duramycin (Molecular Targeting Technologies, Inc., USA), fetal bovine serum (FBS; Gibco, USA), phosphate-buffered saline (PBS; Hyclone, USA), bovine serum albumin (BSA; Hushi, China), Dulbecco's modified Eagle's medium (DMEM; Corning, USA), H₂O₂ (Sigma-Aldrich, USA), FITC-Annexin V

Apoptosis Detection Kit (BD Pharmingen, USA), FACS Calibur (Flow Cytometry, BD Biosciences, USA), N-hydroxysuccinimidyl S-acetylmercaptoacetyltriglycinate (NHS-MAG₃; WuXi AppTec, China), and other reagents were of reagent grade and used as received.

Radiolabeling of [^{99m}Tc]Duramycin and [^{99m}Tc]Annexin V

For Tc-99m labeling of duramycin, we used a single-step kit composed of 15 μg hydrazinonicotinamide (HYNIC)-duramycin as previously reported [21]. Freshly prepared [^{99m}Tc]pertechnetate (277.5 MBq) in 500 μl saline was added to the kit and heated at 80 °C for 20 min. The radiochemical purity was assessed by Radio-TLC with two separate chromatography systems: system 1: silica gel impregnated paper (1 × 10 cm) with 20 % NaCl, in which free [^{99m}Tc]pertechnetate and impurities move to the solvent front, while reduced Tc-99 m and [^{99m}Tc]duramycin stay at the origin; system 2: silica gel impregnated paper (1 × 10 cm) with distilled water, in which free [^{99m}Tc]pertechnetate, impurities, and [^{99m}Tc]duramycin migrate close to the solvent front, while the hydrolyzed reduced Tc-99 m remains at the origin. The radiolabeled method of [^{99m}Tc]linear-duramycin is the same as that of [^{99m}Tc]duramycin.

[^{99m}Tc]Annexin V was prepared as previously reported [25, 26]. Briefly, 25 μg (1 mg/ml) Annexin V was added into a 10K ultrafiltration tube with HEPES buffer (pH 8.0). After vortexing, 1.4 μl (1 mg/ml) of NHS-MAG₃ was added into the tube (the mole ratio of Annexin V and NHS-MAG₃ was 1:5), and then the mixture was incubated at room temperature for 1 h. To remove the excess NHS-MAG₃, ammonium acetate solution (0.25 M, pH 7.0) was added and centrifuged, followed by adding 25 μl tartrate buffer (50 mg/ml, pH 8.0). Finally, 37 MBq freshly prepared [^{99m}Tc]pertechnetate solution and 3 μl SnCl₂·2H₂O solution (1 mg/ml) were added into the mixture and reacted for 20 min at room temperature. For radiochemical purity, two separate chromatography systems were applied as described above with 0.9 % NaCl and 50 % acetonitrile as solvents.

Stability Tests

The *in vitro* stability of radiolabeled duramycin and Annexin V were respectively tested at 1, 3, and 6 h through incubation in 0.1 % BSA, 0.9 % NaCl solution, and DMEM at room temperature and 37 °C. At each time point, radiochemical purity was tested with Radio-TLC.

Cell Culture

RAW264.7 macrophage cells were cultured in DMEM at 37 °C in a humidified atmosphere with 5 % CO₂. Medium

was supplemented with 10 % FBS and 1 % antibiotics (penicillin and streptomycin). Light microscopy was used to check cell viability.

Apoptosis Analysis by Flow Cytometry

For apoptosis assay, cells were treated with a final concentration of 3 mM H₂O₂ in DMEM for 12 h at 37 °C in a humidified atmosphere. Apoptotic cells were measured by flow cytometry after FITC-Annexin V and PI staining according to the manufacturer's instructions. Briefly, cells were washed with PBS and resuspended in binding buffer at a final concentration of 2 × 10⁶ cells/ml. Next, 1 ml of the cell solution was transferred to a 5 ml culture tube, and then 5 μl of FITC-Annexin V and 5 μl of PI were added and incubated for 15 min at room temperature in the dark condition. Finally, 400 μl of binding buffer was added to the culture tube. Untreated cells were used as control.

In Vitro Binding Tests

To study cell affinity of [^{99m}Tc]duramycin, [^{99m}Tc]linear-duramycin, and [^{99m}Tc]Annexin V, RAW264.7 cells were cultured and induced for apoptosis with H₂O₂ [27–29]. Apoptotic cells (2 × 10⁶ cells) were transferred into 5 ml tubes with binding buffer (pH 7.4); then a gradient concentration of radiolabeled Annexin V (1–200 nM), duramycin (1–200 nM), and linear-duramycin (1–200 nM) was respectively added to the tubes at a final volume of 1 ml. After incubation at 37 °C for 2 h, the mixture was centrifuged at 800 r/min for 5 min to remove free radioactivities with the remnant tested as cell-bound radioactivity by using γ-counter (CRC-15R, Capintec Inc., Ramsey, NJ). The same amount of radiolabeled probes was aliquoted in tubes with untreated cells as control groups and also in DMEM solutions without cells to determine nonspecific binding.

Animal Model Establishment

Apolipoprotein E knockout (ApoE^{-/-}) and C57 mice (male, 8 weeks) were purchased from Peking University Laboratory Animal Center (Beijing, China). The ApoE^{-/-} mice were fed with a high-fat diet (HFD, 21 % fat and 0.15 % cholesterol), while the C57 mice were fed a normal murine diet (4–6 % fat and < 0.02 % cholesterol). All mice were fed for at least 20 weeks to establish atherosclerosis before animal experiments.

Micro-SPECT/CT Imaging and Data Analysis

[^{99m}Tc]duramycin (37 MBq/2 μg/mouse) was injected through the tail vein to five ApoE^{-/-} and five C57 mice, while the same dose of [^{99m}Tc]linear-duramycin was

injected into another five ApoE^{-/-} mice. Two hours later, mice were anesthetized *via* inhalation of 2 % isoflurane. Then, mice were placed on a Micro-single-photon emission computed tomography/computed tomography (SPECT/CT) scanner (Bioscan, Washington DC, USA) for SPECT/CT imaging according to the following parameters: CT: tube current, 0.15 mA; tube voltage, 45 keV; exposure time, 500 ms/frame, and frame resolution, 256 × 512; SPECT: energy peak, 140 keV; scanning time, 35 s/projection; window width, 10 %; resolution, 1 mm/pixel; and matrix, 256 × 256. SPECT and CT scanning were performed with same bed position. Data were reconstructed using the HiSPECT algorithm. One week later, those mice that experienced [^{99m}Tc]duramycin SPECT/CT underwent micro-SPECT/CT imaging again with same parameters at 5 h after injection of [^{99m}Tc]Annexin V (37 MBq/25 μg/mouse) through tail vein.

All reconstructed data was used to post-processing with software InVivoScope (Version 1.43, Bioscan, Washington DC, USA). For quantitative analysis, 3D region of interest (ROI) was drawn in the place of the thoracic aorta with obvious radioactivity accumulation in each mouse, while the background ROIs with similar diameter were drawn in the area of surrounding muscle. Concentration of radioactivity of each ROI (μCi/mm³) was calculated by the software. The plaque-to-background ratio (P/B) was used to express plaque signal intensity, aiming to reduce inter-mice variations.

Aorta Harvest

After micro-SPECT/CT imaging, mice were anesthetized by intraperitoneal injection of 4 % chloral hydrate. Weight were measured and recorded. Then aortas were perfused with 0.9 % NaCl and fixed with 4 % paraformaldehyde, respectively, through a puncture in the left ventricle. After that, the entire aorta was exposed and photographed with a digital camera for visualizing lipid deposition. Finally, aortas were harvested and stored in the 20 % sucrose solution for use after fixing in 4 % paraformaldehyde at 4 °C overnight.

Oil Red O Staining

Oil Red O was used to stain lipids deposited in atherosclerosis plaques. Briefly, the dissected aortas were opened longitudinally and incubated in 60 % propylene glycol for 10 min. Then, the aortas were stained in 0.5 % Oil Red O solution for 30 min and washed with 60 % propylene glycol for 5 min until the background was nearly transparent. The stained aorta was placed flat on a black board for imaging using a digital camera. Images were then transferred to Image Pro Plus (Version 6.0, Media Cybernetics, Washington DC, USA) to calculate the percentages of area that were stained positive.

Histology and Immunohistochemistry

Paraformaldehyde-fixed aortas were embedded in paraffin and sectioned at 5 μm thickness at thoracic regions with obvious plaques. Sections were stained with hematoxylin-eosin (HE) for morphologic analysis. In order to look insight into the plaques, CD68 staining and the terminal deoxynucleotidyl transferase-mediated UTP end labeling (TUNEL) were performed on adjacent sections according to a standard procedure using a commercially available kit. The apoptotic cells presented as tan particles were considered as positive cells in TUNEL images. CD68-staining and TUNEL images were analyzed by Image Pro Plus. Integrated Optic Density/Area (IOD/Area) and Apoptosis Index

(AI) were used to express the quantification of macrophages and apoptotic cells in plaques, respectively.

Statistical Analysis

SPSS 22 (IBM, Chicago, IL, USA) and GraphPad Prism 6.0 (GraphPad Software Inc.) were used for statistical analysis. Numeric parameters were presented as mean \pm standard deviation (s.d.). To determine the statistical significance of differences between groups, a one-way ANOVA followed by a Bonferroni post-hoc test was performed. The correlation between P/B on

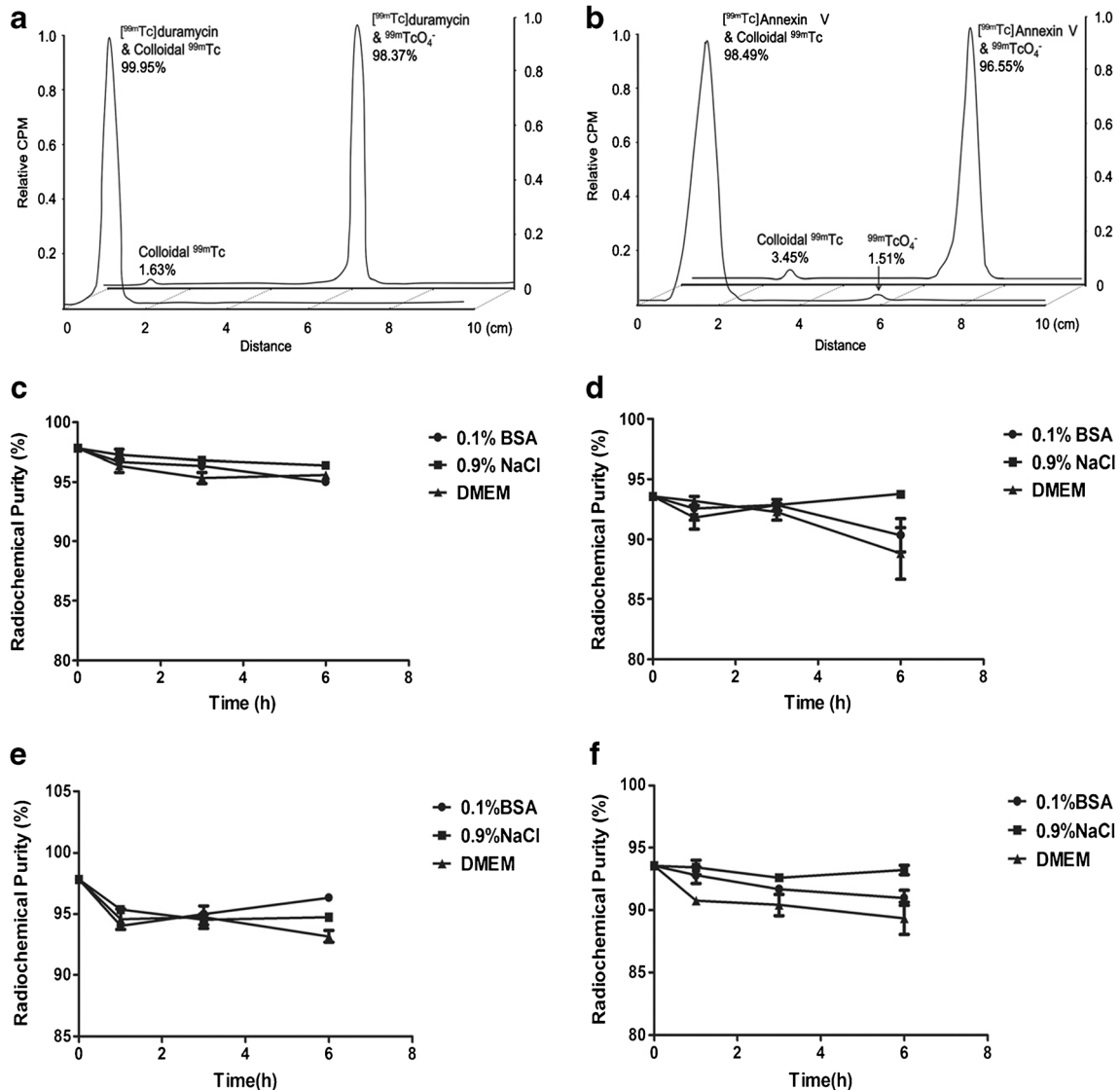


Fig. 1. Radiochemistry and *in vitro* stability of [^{99m}Tc]duramycin and [^{99m}Tc]Annexin V: radiochemical purities of **a** [^{99m}Tc]duramycin and **b** [^{99m}Tc]Annexin V evaluated by Radio-TLC. Stability of [^{99m}Tc]duramycin and [^{99m}Tc]Annexin V in 0.1 % BSA, 0.9 % NaCl, and DMEM for 6 h post-labeling: Stability of **c** [^{99m}Tc]duramycin and **d** [^{99m}Tc]Annexin V at room temperature; stability of **e** [^{99m}Tc]duramycin and **f** [^{99m}Tc]Annexin V at 37 °C.

[^{99m}Tc]duramycin or [^{99m}Tc]Annexin V SPECT/CT and AI in plaque of corresponding area was calculated by Pearson correlation analysis. *P* value < 0.05 was considered statistically significant.

Results

Radiolabeling and Stability of [^{99m}Tc]Duramycin and [^{99m}Tc]Annexin V

The radiochemical purities of [^{99m}Tc]duramycin and [^{99m}Tc]Annexin V were 97.13 ± 1.52 % (*n* = 3, Fig. 1a) and 94.94 ± 0.65 % (*n* = 3, Fig. 1b), respectively. The final radiopharmaceuticals with high purity were used for further *in vitro* and *in vivo* studies without additional purification. The specific radioactivity of [^{99m}Tc]duramycin and [^{99m}Tc]Annexin V was 3.7×10^{10} and 4.736×10^{10} MBq/mol, respectively. The stability of Tc-99 m labeled probes was further evaluated at room temperature and 37 °C in 0.1 % BSA, 0.9 % NaCl, and DMEM, respectively, resulting in over 94 % stability for [^{99m}Tc]duramycin (Fig. 1c, e) and

over 90 % stability for [^{99m}Tc]Annexin V (Fig. 1d, f) over a 6-h post-labeling period.

In Vitro Affinity to Apoptotic Cells

The apoptotic ratio of untreated (Fig. 2a) and H₂O₂-induced (Fig. 2b) cells was evaluated by flow cytometry with FITC-Annexin V. As shown in Fig. 2c, the apoptotic ratio of normal cells was 3.61 ± 0.44 %, which was significantly lower (*n* = 3, mean ± s.d., *P* < 0.05) than the H₂O₂-treated cells (22.60 ± 2.92 %). A cell binding test revealed that the total binding capacity (Bmax) of duramycin is about $56.04 \text{ mol}/10^{19}$ cells (Fig. 2d), which is about 1.78-fold higher than that of Annexin V (Bmax = $31.55 \text{ mol}/10^{19}$ cells; Fig. 2e). The equilibrium dissociation constant (Kd) was calculated to be 6.92 nM for duramycin and 12.63 nM for Annexin V, respectively. The cell binding curve of [^{99m}Tc]linear-duramycin to apoptotic cells over concentrations was close to the baseline, while [^{99m}Tc]duramycin revealed high specificity to the apoptotic cells (Fig. 2d), which was even higher than the specificity of [^{99m}Tc]Annexin V (Fig. 2e). The affinity of

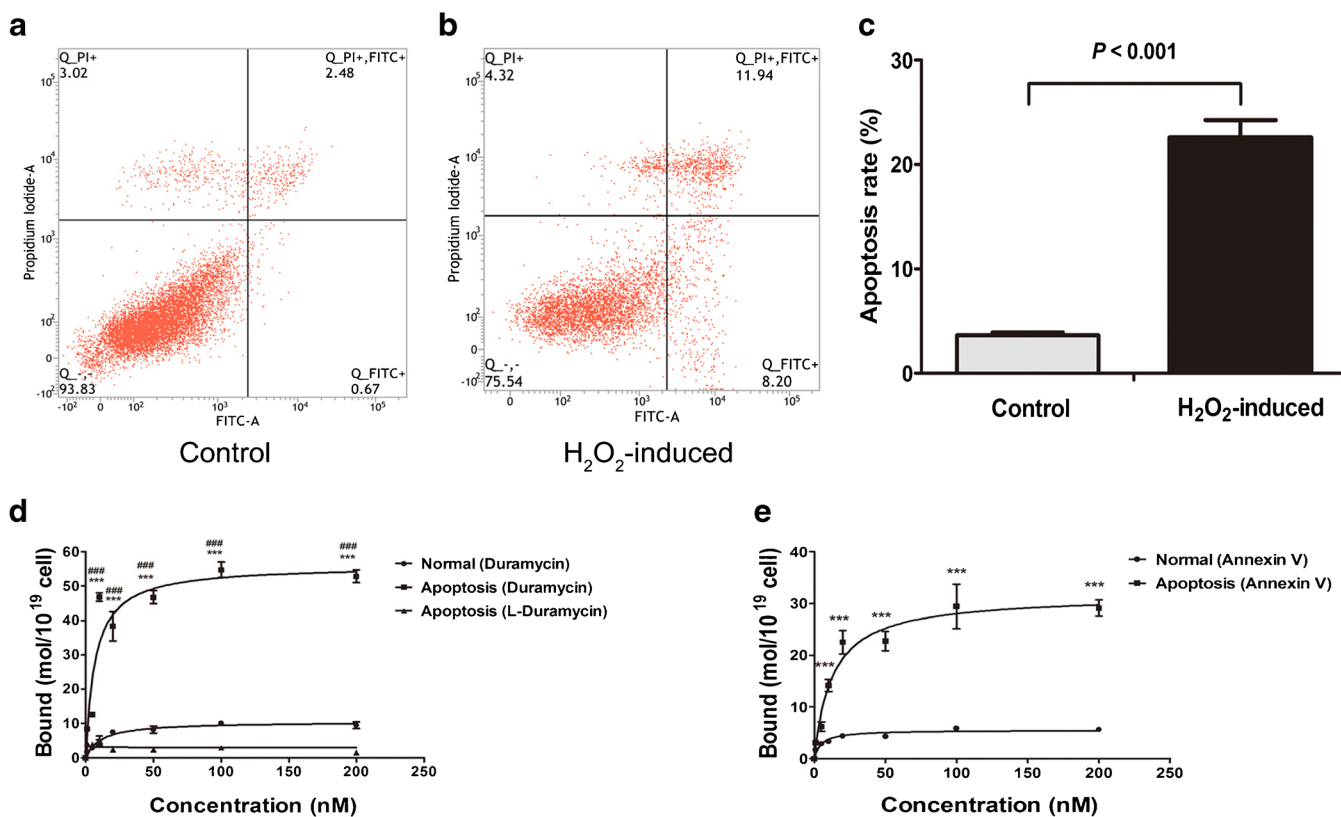


Fig. 2. *In vitro* cell binding of [^{99m}Tc]duramycin and [^{99m}Tc]Annexin V to apoptotic cells: RAW264.7 cells were incubated in medium **a** without any stimulation for 12 h at 37 °C resulted in lower percentage of apoptosis than those that were **b** treated with 3 μM H₂O₂, as detected by flow cytometry analysis. **c** Quantitative statistical comparison of the percentage of apoptosis between H₂O₂-induced group and normal group (*n* = 3, mean ± s.d., ****P* < 0.001). Cell binding curves with gradient concentrations of **d** [^{99m}Tc]duramycin and **e** [^{99m}Tc]Annexin V with apoptotic cells and normal cells, respectively (*n* = 3, mean ± s.d., ****P* < 0.001). A significant difference was also found between [^{99m}Tc]duramycin and [^{99m}Tc]linear-duramycin in apoptotic cell binding (*n* = 3, mean ± s.d., ****P* < 0.001).

[^{99m}Tc]duramycin to normal cells was significantly lower compared with results from H₂O₂-induced cells, and slightly higher than [^{99m}Tc]linear-duramycin ($n = 3$, mean \pm s.d., $^{***}P < 0.001$, $^{####}P < 0.001$).

In Vivo Imaging of Atherosclerosis

SPECT/CT was used to image atherosclerotic lesions using [^{99m}Tc]duramycin, [^{99m}Tc]linear-duramycin, and

[^{99m}Tc]Annexin V. As presented in Fig. 3, the radioactivity of plaques increased progressively with age in ApoE^{-/-} mice: P/B of 8.23 ± 0.91 at 20 weeks (Fig. 3a) and 15.02 ± 0.23 at 30 weeks (Fig. 3f) for [^{99m}Tc]duramycin, and P/B of 5.45 ± 0.48 at 20 weeks (Fig. 3d) and 12.14 ± 0.22 at 30 weeks (Fig. 3i) for [^{99m}Tc]Annexin V. Interestingly, the P/B of [^{99m}Tc]duramycin was higher than that of [^{99m}Tc]Annexin V over the period of monitoring for 30 weeks ($n = 3$, mean \pm s.d., $P < 0.05$; Fig. 3k). The uptake levels of both tracers in ApoE^{-/-} mice were noticeably

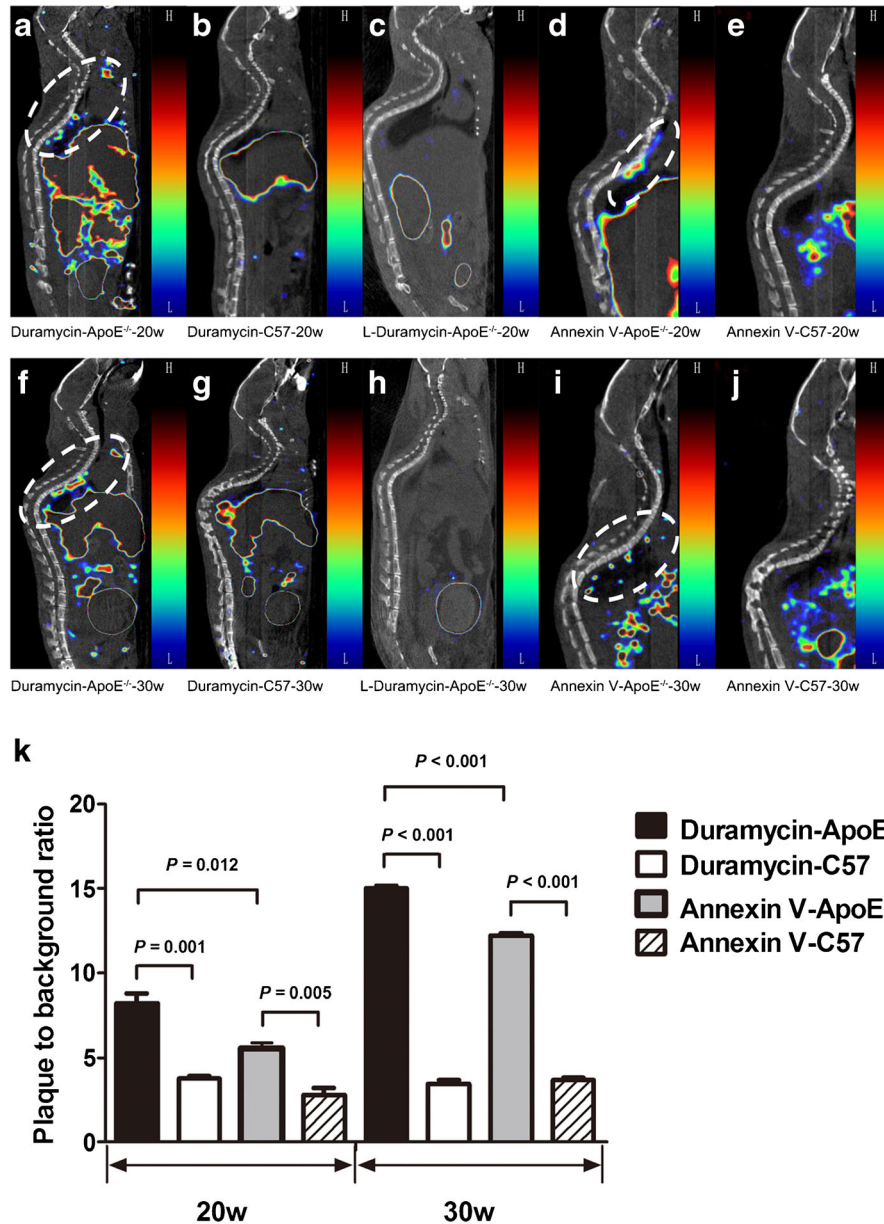


Fig. 3. Micro-SPECT/CT imaging and corresponding quantitative analysis: sagittal SPECT/CT images of 20 w ApoE^{-/-} mice scanned at 2 h post-injection of **a** [^{99m}Tc]duramycin and **c** [^{99m}Tc]linear-duramycin, and **d** scanned at 5 h post-injection of [^{99m}Tc]Annexin V. The control 20 weeks C57 mice were **b** scanned at 2 h post-injection of [^{99m}Tc]duramycin and **e** scanned at 5 h post-injection of [^{99m}Tc]Annexin V. **f-j** Sagittal SPECT/CT images of 30 weeks mice acquired with the same tracers and order as shown in **a-e**. **k** Quantitative analysis of P/B on SPECT/CT: ApoE^{-/-} mice represented higher uptake of both [^{99m}Tc]duramycin and [^{99m}Tc]Annexin V than control C57 mice within the same age groups ($n = 3$, mean \pm s.d.). In ApoE^{-/-} mice, [^{99m}Tc]duramycin showed significantly higher uptake compared with [^{99m}Tc]Annexin V ($n = 3$, mean \pm s.d.).

higher than those in C57 mice, and higher than the control [^{99m}Tc]linear-duramycin uptake in ApoE^{-/-} mice ($n = 3$, mean \pm s.d., $P < 0.05$; Fig. 3k).

Ex Vivo Lipid Deposition in Plaques Confirmed In Vivo Imaging

Color images in Fig. 4a–d shown that atherosclerotic plaques were predominantly located in the thoracic aortas of ApoE^{-/-} mice, while no plaques were observed in C57 mice. Despite substantial increase of body weight in both ApoE^{-/-} and C57 mice from 20 to 30 weeks, ApoE^{-/-} mice showed significant higher increase than C57 mice (Fig. 4i). Oil Red O staining of aortas replicated these findings, as shown in Fig. 4e–i. The percentage of plaque area in ApoE^{-/-} mice at 20 and 30 weeks was 23.02 ± 1.98 and 55.00 ± 1.95 %, respectively, which is significantly higher than those of C57 mice either at 20 weeks (1.30 ± 0.37 %) or at 30 weeks (1.30 ± 0.25 %). Besides, the plaque area of ApoE^{-/-} mice increased significantly from 20 to 30 weeks ($P < 0.001$), while those of C57 mice did not show significant difference between the two time points ($P > 0.05$).

Apoptosis and Macrophage Infiltration in Atherosclerotic Plaques

HE staining of ApoE^{-/-} mice revealed that a significant amount of plaques was developed during 20 and 30 weeks (Fig. 5a, d). To evaluate macrophage infiltration in the atherosclerotic plaques, CD68 staining was further used in addition to TUNEL assay for *in situ* apoptosis in plaques. As demonstrated by CD68 staining, the macrophage infiltration in ApoE^{-/-} at 30 weeks (IOD/Area, 0.135 ± 0.019) was more severe than those at 20 weeks (IOD/Area, 0.053 ± 0.016 ; $P = 0.005$) (Fig. 5b, e, j). Interestingly, significantly more TUNEL-positive cells were observed in ApoE^{-/-} mice at 30 weeks than those of 20 weeks old ApoE^{-/-} mice in the CD68 positive area (expressed as AI, 23.06 ± 7.40 vs. 7.42 ± 1.63 , $P = 0.023$; Fig. 5c, f, k). These results indicate that macrophage infiltration and apoptosis in atherosclerotic plaques might deteriorate along with the progress of plaque. However, no meaningful findings could be observed in C57 mice on HE, CD68, and TUNEL staining (Fig. 5g–i). The Pearson correlation analysis further proved that plaque radioactivity of [^{99m}Tc]duramycin and [^{99m}Tc]Annexin V significantly correlated with the corresponding AI in TUNEL ($r = 0.976$ and

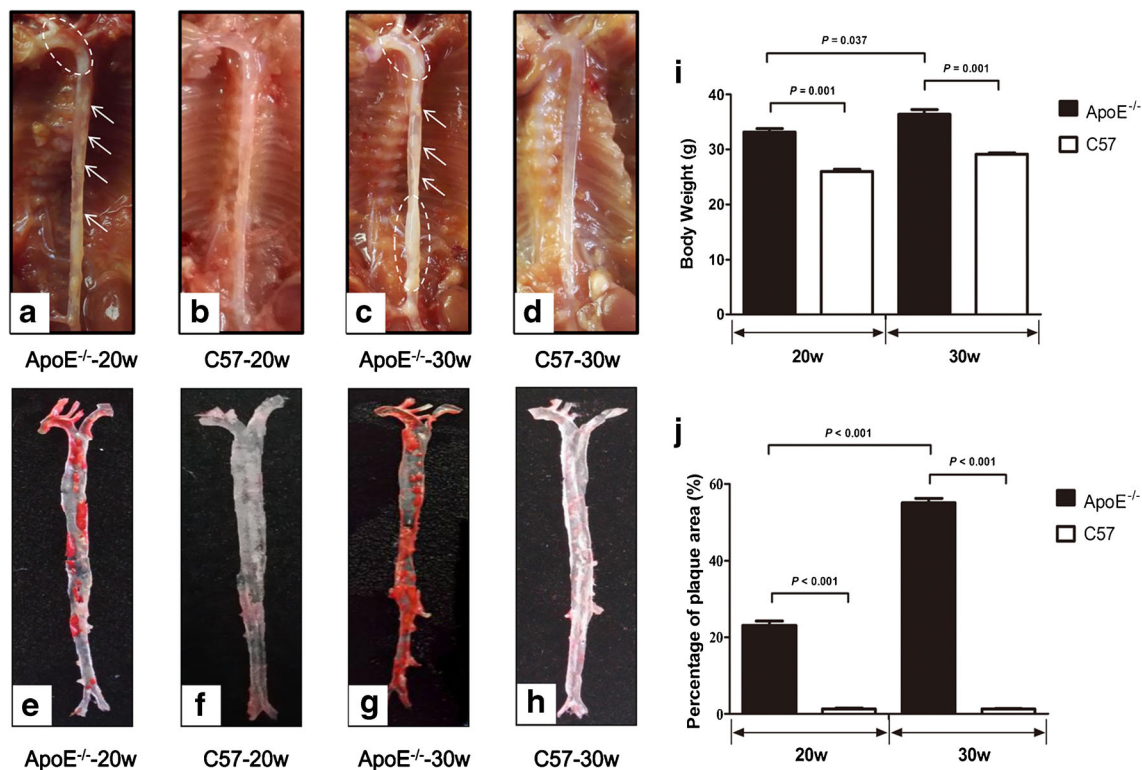


Fig. 4. Lipid location in atherosclerotic plaques: representative images of exposed aortas of a, c ApoE^{-/-} mice and b, d C57 mice at a, b 20 weeks and c, d 30 weeks show obvious lipid deposition in ApoE^{-/-} mice (circles and arrows) but not in C57 mice. e–h Oil Red O staining images of aortas resected from the mice corresponding to a–d in order. Lipids deposited in plaques were stained in red. i Body weight analysis between mice groups ($n = 3$, mean \pm s.d., $P = 0.001$ between ApoE^{-/-} and C57 mice within the same age group; $P = 0.037$ between 20 and 30 weeks ApoE^{-/-} mice) and j quantitative analysis of plaques in aorta measured by Oil Red staining from e to h ($n = 3$, mean \pm s.d., $P < 0.001$ between ApoE^{-/-} and C57 mice within the same age group; $P < 0.001$ between 20 and 30 weeks ApoE^{-/-} mice).

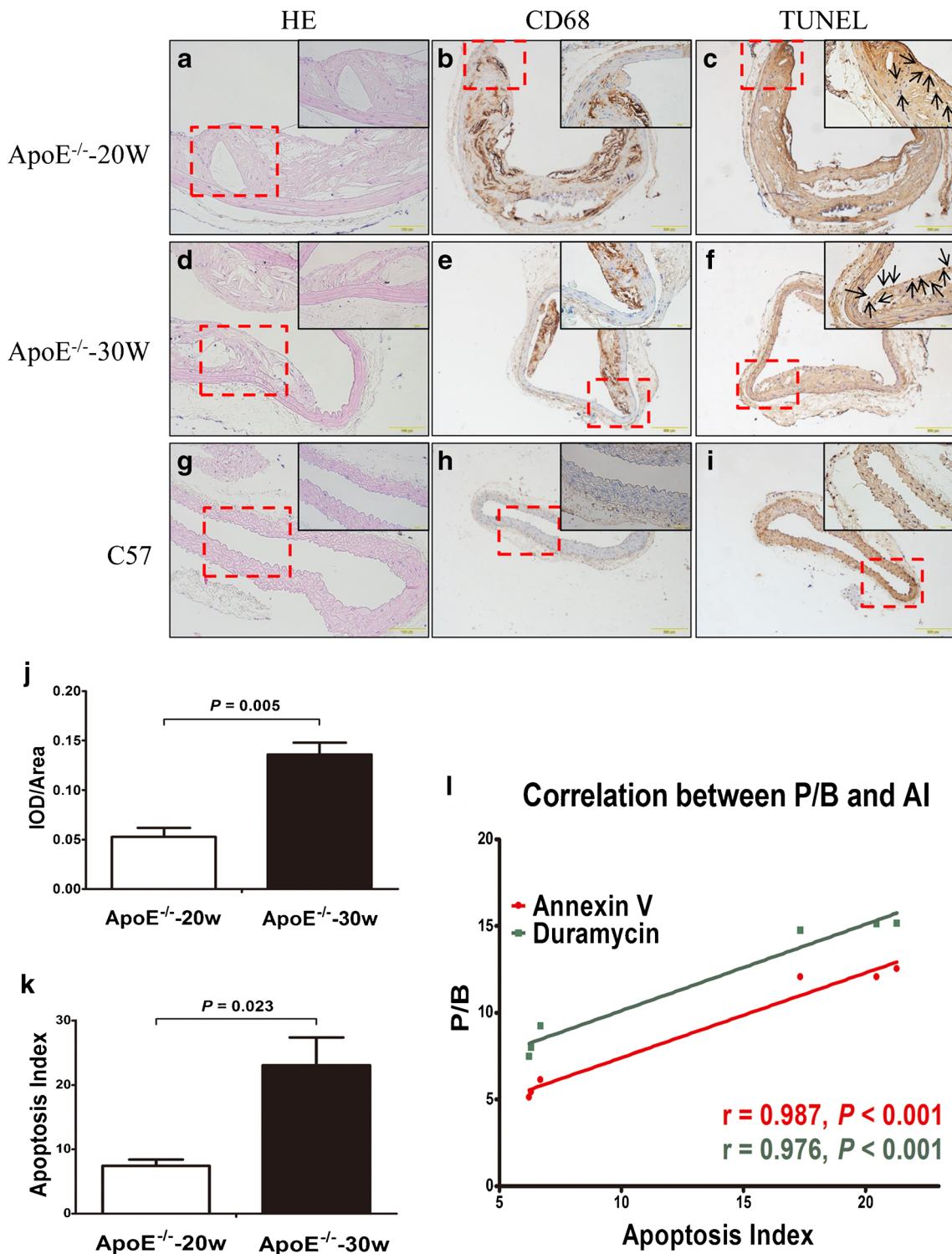


Fig. 5. Pathology and immunohistochemistry of aortic tissues from ApoE^{-/-} mice: **a-f** microscopic images of HE (×200), CD68 (×100), and TUNEL (×100) staining of aortic tissues obtained from 20 and 30 weeks old ApoE^{-/-} mice. **g-i** C57 aortas were used as control. *Insets* are microscopic images captured with higher magnification (×400) of corresponding staining. In TUNEL staining, apoptotic cells are stained *brown* (*black arrows*). Data analysis of **j** CD68 and **k** TUNEL staining of aortic tissue obtained from ApoE^{-/-} mice between 20 and 30 weeks ($n = 6$, mean ± s.d.). **l** Pearson correlation analysis between P/B on SPECT/CT and corresponding AI in TUNEL. *IOD*, integrated optic density; *AI*, apoptosis index.

0.987, respectively; Fig. 5l). This indicates that both [^{99m}Tc]duramycin and [^{99m}Tc]Annexin V could be used as

reliable SPECT/CT imaging agents for evaluating macrophage infiltration and apoptosis in unstable atherosclerotic

plaques. However, no plaques were seen in C57 mice by HE, CD68, or TUNEL staining (Fig. 5g–i).

Discussion

Although Annexin V has been extensively studied to monitor apoptotic environment in many disease models including myocarditis and infective endocarditis, tumors, and myocardial ischemia, there are several limitations in evaluating unstable atherosclerotic plaques compared with duramycin [13, 15–20].

First, the size of targeting moiety matters. Annexin V is a human protein with relative larger molecular weight (36 kDa), while duramycin contains only 19 amino acids with molecular weight of 2 kDa. This means duramycin is more permeable to the tissue of interest than Annexin V, which contributes to a higher targeting efficiency [30]. In the cell binding test (Fig. 2), [^{99m}Tc]duramycin showed a relatively lower Kd value (6.92 nM), thus a higher binding affinity, compared with [^{99m}Tc]Annexin V (12.63 nM) in binding to apoptotic macrophages. Additionally, because of the relative large size, Annexin V presents slow clearance from the background tissue and non-targeted organs, leading to reduced signal-to-background ratio [22]. Both of tracers' renal excretion is the predominant route of clearance, but the blood clearance is faster with duramycin than with Annexin V (blood half-life of less than 4 vs 10.5 min) [9, 13, 21]. This also proved by micro-SPECT/CT scans of ApoE^{-/-} mice after injecting [^{99m}Tc]duramycin and [^{99m}Tc]Annexin V. [^{99m}Tc]Annexin V SPECT/CT showed a high background uptake at 2 h post-injection, leading to a lower radioactivity uptake in the plaques, while higher P/B ratio was obtained at 5 h post-injection. In contrast, [^{99m}Tc]duramycin depicted a high uptake in the

plaques with fast clearance from the background, thus resulted in a higher P/B ratio at 2 h post-injection (Fig. 6).

Second, target density (Bmax) and the affinity (Kd) of tracer on the target tissue matter. PE and PS show a synchronized externalization when cells experience apoptosis [10], and importantly, PE is the second most abundant phospholipid with the PE/PS ratio of 2.5–4.0 in mammalian plasma membrane [31, 32]. The Bmax of [^{99m}Tc]duramycin (56.04 mol/10¹⁹ cell) was higher than that of [^{99m}Tc]Annexin V (31.55 mol/10¹⁹ cell) in binding to apoptotic cells. In addition, *in vivo* SPECT/CT imaging proved higher affinity of [^{99m}Tc]duramycin on the plaques compared with [^{99m}Tc]Annexin V in ApoE^{-/-} mice ($P < 0.05$; Fig. 3). In normal cells, the binding of [^{99m}Tc]duramycin was higher than [^{99m}Tc]Annexin V (Fig. 2). It has been well documented that outer layer of normal cells contains PE, while no PS detected [31]. However, there is no significantly nonspecific uptake was seen in SPECT/CT images (Fig. 3).

Next, specificity should be considered. PS exposure onto the cell surface is not only presented during apoptosis, but also occurs in activated macrophages and autophagy, thus cells expressing PS can be cleared by macrophages before the imaging probe can target these cells [33, 34]. In addition, duramycin only binds to PE, whereas Annexin V interacts with PS, PI, and likely PE as well [35]. In order to confirm the high affinity and specificity of [^{99m}Tc]duramycin, we chose inactivated duramycin (linear-duramycin) as control, which resulted in little to no binding to the target tissue *in vitro* and *in vivo* (Figs. 2 and 3). The regions showing high uptake of [^{99m}Tc]duramycin rather than [^{99m}Tc]linear-duramycin were filled with apoptotic macrophages as detected by TUNEL and CD68 staining (Fig. 5).

Nevertheless, there are several limitations that need to be improved. [^{99m}Tc]duramycin and [^{99m}Tc]Annexin V SPECT/CT only demonstrated atherosclerotic plaques in

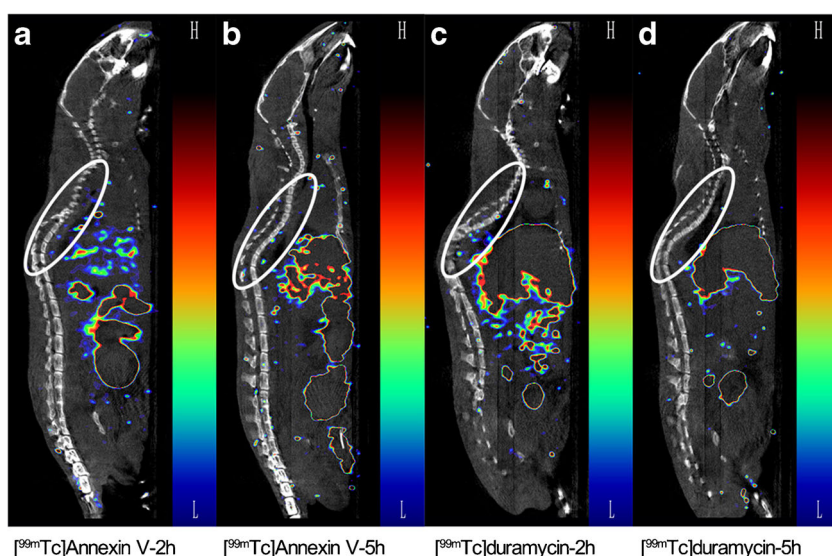


Fig. 6. Explore the micro-SPECT/CT imaging time of [^{99m}Tc]Annexin V and [^{99m}Tc]duramycin: [^{99m}Tc]Annexin V images in ApoE^{-/-} mice at **a** 2 h and **b** 5 h. The uptake of [^{99m}Tc]Annexin V in aorta at 5 h is higher than that at 2 h, while the background is lower (*white circle*). [^{99m}Tc]duramycin images in ApoE^{-/-} mice at **c** 2 h and **d** 5 h. [^{99m}Tc]duramycin has a significantly uptake in ApoE^{-/-} mice at 2 h (*white circle*), and it has been cleared out from the aorta at 5 h.

thoracic aorta, whereas plaques could be visualized throughout the whole aorta either in the digital camera imaging or in Oil Red O staining. This might be resulted from the lower radioactivity uptake in abdominal aorta, which might have been covered by surrounding high radioactivity from the liver or kidney. The hepatobiliary and intestinal signal may hinder the detection of plaques in abdominal aorta [24]. Additionally, the present study does not include *in vivo* pharmacokinetic and biodistribution experiments of both tracers, which were already reported previously [9, 13, 18, 22, 30, 36–38]. The mouse model we used just mimicked the process of atherosclerosis, but the pathogenesis of plaques in human is more complex, there could be a discrepancy in clinical transformation.

Additionally, as it was shown in Fig. 6, we can find [^{99m}Tc]Annexin V has longer effective image time window compared to [^{99m}Tc]duramycin. There are similar focus uptakes in images achieved at 2 h p.i. (Fig. 6a, c); however, [^{99m}Tc]Annexin V was showing more intense signal at 5 h p.i. compared to [^{99m}Tc]duramycin (Fig. 6b, d). There were other studies that also proved that Annexin V could be labeled with long half-life radionuclide such as I-124 and In-111 for detecting longer-term biological process and effectively capturing the minimal apoptotic cells [39, 40]. Thus, Annexin V as a conventional apoptotic imaging agent still plays its unique role in some certain diseases and evaluation of prognosis.

Conclusion

The study showed that [^{99m}Tc]duramycin was comparable to [^{99m}Tc]Annexin V with regard to the cell binding affinity and specificity *in vitro*, as well as the plaque-to-background ratio of SPECT/CT imaging in detecting apoptosis in atherosclerosis in early time points, holds promise for effective apoptotic imaging by monitoring vulnerable atherosclerotic plaques. However, Annexin V has its advantage on imaging at longer time points after injection when it was labeled by longer half-time isotopes, such as Cu-64, I-124, and Zr-89.

Acknowledgments. Funding support from The National Nature Science Foundation of China (81471706, and 81671735) and The Shanghai Science and Technology Committee International Collaboration Project (16410722700) is gratefully appreciated. The authors are grateful to technical supports from Prof. Yingjian Zhang and Dr. Jianping Zhang from Center for Biomedical Imaging, Fudan University, and Shanghai Engineering Research Center of Molecular Imaging Probes.

Author Contributions. Y.H., G.B.L., and D.F.C participated in the experimental and data analysis. Y.H. wrote the manuscript. Y.H., G.B.L., Y.L.L., and H.Z. involved in animal imaging and dealt with the aortas. B.G, K.P, and H.S.C. helped in polishing the articles. Y.H., D.F.C., and H.C.S designed and controlled the quality of study. All authors have reviewed the manuscript.

Compliance with Ethical Standards

Conflict of Interest

Brian D Gray and Koon Y Pak are employees of Molecular Targeting Technologies, Inc. All other authors declare that there is no conflict of

interest regarding the publication of this paper. At all times, the other authors had full control over study data and interpretation.

References

- Joshi NV, Vesey AT, Williams MC et al (2014) [¹⁸F]fluoride positron emission tomography for identification of ruptured and high-risk coronary atherosclerotic plaques: a prospective clinical trial. *Lancet* 383:705–713
- van Tilborg GAF, Vucic E, Strijkers GJ et al (2010) Annexin A5-functionalized bimodal nanoparticles for MRI and fluorescence imaging of atherosclerotic plaques. *Bioconjugate Chem* 21:1794–1803
- Leung K (2004) [^{99m}Tc]Tricarboxyl-His6-annexin A5. <https://www.ncbi.nlm.nih.gov/books/NBK98866/>
- Tepper CG, Studzinski GP (1993) Resistance of mitochondrial DNA to degradation characterizes the apoptotic but not the necrotic mode of human leukemia cell death. *J Cell Biochem* 52:352–361
- Knezevic T, Myers VD, Gordon J et al (2015) BAG₃: a new player in the heart failure paradigm. *Heart Fail Rev* 20:423–434
- De Saint-Hubert M, Bauwens M, Deckers N et al (2014) *In vivo* molecular imaging of apoptosis and necrosis in atherosclerotic plaques using microSPECT-CT and microPET-CT imaging. *Mol Imaging Biol* 16:246–254
- Figg NL, Bennett MR (2015) Quantification of apoptosis in mouse atherosclerotic lesions. *Methods Mol Biol* 1339:191–199
- Daleke DL (2003) Regulation of transbilayer plasma membrane phospholipid asymmetry. *J Lipid Res* 44:233–242
- Johnson SE, Li Z, Liu Y et al (2013) Whole-body imaging of high-dose ionizing irradiation-induced tissue injuries using [^{99m}Tc]duramycin. *J Nucl Med* 54:1397–1403
- Zhao M (2011) Lantibiotics as probes for phosphatidylethanolamine. *Amino Acids* 41:1071–1079
- Isobe S, Tsimikas S, Zhou J et al (2006) Noninvasive imaging of atherosclerotic lesions in apolipoprotein E-deficient and low-density-lipoprotein receptor-deficient mice with annexin A5. *J Nucl Med* 47:1497–1505
- Subbarayan M, Hafeli UO, Feyes DK et al (2003) A simplified method for preparation of [^{99m}Tc]annexin V and its biologic evaluation for *in vivo* imaging of apoptosis after photodynamic therapy. *J Nucl Med* 44(4):650–656
- Benali K, Louedec L, Azzouna R B, et al. (2014) Preclinical validation of [^{99m}Tc]annexin A5-128 in experimental autoimmune myocarditis and infective endocarditis: comparison with [^{99m}Tc]HYNIC-annexin A5. *Mol Imaging* 13
- Lu C, Jiang Q, Hu M et al (2013) Preliminary biological evaluation of novel [^{99m}Tc]Cys-Annexin A5 as a apoptosis imaging agent. *Molecules* 18:6908–6918
- Cheng D, Li X, Zhang C et al (2015) Detection of vulnerable atherosclerosis plaques with a dual-modal single-photon-emission computed tomography/magnetic resonance imaging probe targeting apoptotic macrophages. *ACS Appl Mater Interfaces* 7:2847–2855
- Burgmaier M, Schutters K, Willems B et al (2014) AnxA5 reduces plaque inflammation of advanced atherosclerotic lesions in apoE^{-/-} mice. *J Cell Mol Med* 18:2117–2124
- Zhao Y, Watanabe A, Zhao S et al (2014) Suppressive effects of irbesartan on inflammation and apoptosis in atherosclerotic plaques of apoE^{-/-} mice: molecular imaging with [¹⁴C]FDG and [^{99m}Tc]Annexin A5. *PLoS One* 9:e89338
- Ogawa K, Ohtsuki K, Shibata T et al (2013) Development and evaluation of a novel Tc-99m labeled Annexin A5 for early detection of response to chemotherapy. *PLoS One* 8:e81191
- Tian R, Pan D (2012) Imaging myocardial ischemia and reperfusion injury via Cy5.5-Annexin V. *Nucl Med Mol Imaging* 46:155–161
- Li X, Wang C, Tan H et al (2016) Gold nanoparticles-based SPECT/CT imaging probe targeting for vulnerable atherosclerosis plaques. *Biomaterials* 108:71–80
- Zhao M, Li Z, Bugenhagen S (2008) Tc-99m labeled duramycin as a novel phosphatidylethanolamine-binding molecular probe. *J Nucl Med* 49:1345–1352
- Elvas F, Vangestel C, Rapic S et al (2015) Characterization of [^{99m}Tc]duramycin as a SPECT imaging agent for early assessment of tumor apoptosis. *Mol Imaging Biol* 17:838–847

23. Zhang Y, Stevenson GD, Barber C et al (2013) Imaging of rat cerebral ischemia-reperfusion injury using Tc-99m labeled duramycin. *Nucl Med Biol* 40:80–88
24. Liu Z, Larsen BT, Lerman LO et al (2016) Detection of atherosclerotic plaques in ApoE-deficient mice using [^{99m}Tc]duramycin. *Nucl Med Biol* 43:496–505
25. Wang Y, Liu G, Hnatowich DJ (2006) Methods for MAG₃ conjugation and Tc-99m radiolabeling of biomolecules. *Nat Protoc* 1:1477–1480
26. Wang Y, Liu X, Hnatowich DJ (2007) An improved synthesis of NHS-MAG₃ for conjugation and radiolabeling of biomolecules with Tc-99m at room temperature. *Nat Protoc* 2:972–978
27. Kim MJ, Jeong HJ, Kim DW et al (2014) PEP-1-PON1 protein regulates inflammatory response in raw 264.7 macrophages and ameliorates inflammation in a TPA-induced animal model. *PLoS ONE* 9:e86034
28. Laochumroonvorapong P, Paul S, Elkon KB et al (1996) H₂O₂ induces monocyte apoptosis and reduces viability of *Mycobacterium avium-M. intracellulare* within cultured human monocytes. *Infect Immun* 64:452–459
29. Tyurin VA, Balasubramanian K, Winnica D et al (2014) Oxidatively modified phosphatidylserines on the surface of apoptotic cells are essential phagocytic ‘eat-me’ signals: cleavage and inhibition of phagocytosis by Lp-PLA2. *Cell Death Differ* 21:825–835
30. Audi S, Li Z, Capacete J et al (2012) Understanding the in vivo uptake kinetics of a phosphatidylethanolamine-binding agent [^{99m}Tc]duramycin. *Nucl Med Biol* 39:821–825
31. Fadeel B, Xue D (2009) The ins and outs of phospholipid asymmetry in the plasma membrane: roles in health and disease. *Crit Rev Biochem Mol* 44:264–277
32. Post JA, Verkleij AJ, Langer GA (1995) Organization and function of sarcolemmal phospholipids in control and ischemic/reperfused cardiomyocytes. *J Mol Cell Cardiol* 27:749–760
33. Callahan MK, Williamson P, Schlegel RA (2000) Surface expression of phosphatidylserine on macrophages is required for phagocytosis of apoptotic thymocytes. *Cell Death Differ* 7:645–653
34. Ogawa K, Aoki M (2014) Radiolabeled apoptosis imaging agents for early detection of response to therapy. *Sci World J* 2014:1–11
35. Marconescu A, Thorpe PE (2008) Coincident exposure of phosphatidylethanolamine and anionic phospholipids on the surface of irradiated cells. *BBA-Biomembranes* 1778:2217–2224
36. Zhao M, Li Z (2012) A single-step kit formulation for the Tc-99m labeling of HYNIC-duramycin. *Nucl Med Biol* 39:1006–1011
37. Zhang R, Lu W, Wen X et al (2011) Annexin A5-conjugated polymeric micelles for dual SPECT and optical detection of apoptosis. *J Nucl Med* 52:958–964
38. Wang L, Wang F, Fang W et al (2015) The feasibility of imaging myocardial ischemic/reperfusion injury using Tc-99m labeled duramycin in a porcine model. *Nucl Med Biol* 42:198–204
39. Ke S, Wen X, Wu Q et al (2004) Imaging taxane-induced tumor apoptosis using PEGylated, in-111 labeled Annexin V. *J Nucl Med* 45:108
40. Glaser M, Collingridge DR, Aboagye EO et al (2003) Iodine-124 labeled annexin-V as a potential radiotracer to study apoptosis using positron emission tomography. *Appl Radiat Isot* 58:55–62